Green Chemistry

PAPER

View Article Online
View Journal | View Issue

Cite this: *Green Chem.*, 2025, **27**, 1696

Natural wood as a lithium metal host†

Wei-Jing Chen, *[a] Shang-Jie Yu,[a] Qian Sun,[b] Xin Shen,[c] Peng Shi,[d] Tong-Qi Yuan *[b] and Zhaoqing Lu*[a]

Received 31st October 2024,
Accepted 10th January 2025

DOI: 10.1039/d4gc05507a

rsc.li/greenchem

Lithium metal stands out as an advanced anode material for next-generation rechargeable high-energy-density batteries. Nevertheless, the non-uniform behavior of Li plating/stripping causes severe dendrite growth and volume expansion, inducing rapid lifespan decay and even safety hazards. Introducing a Li host with a three-dimensional (3D) structure and interconnecting pores has been proven effective for solving these issues. In this contribution, natural wood, which possesses an exquisite 3D interconnected hierarchical porous structure, is employed as a Li host. The wood host facilitates homogenization of the electric field intensity near the Li anode, thereby regulating the homogeneity during Li plating/stripping. As demonstrated in Li|Cu half cells, the wood host enables 66 cycles with a coulombic efficiency retention of 80%, surpassing the mere 25 cycles achievable without the host. Furthermore, the wood/Li composite anode exhibits reduced polarizations and extended cycling lifespans in both Li|LFP and Li|S full coin cells. Leveraging the unique characteristics of the natural wood structure, an all-wood-based Li|S full coin cell is also assembled. This study not only illuminates the promise of wood as a material for optimizing Li anode performance, but also offers valuable insights for the design of structures for materials used in rechargeable batteries.

Green foundation

1. There is increasing interest in utilizing environmentally friendly biomass as a replacement for fossil-derived materials in batteries. In this study, wood, a typical biomass material characterized by its intricate three-dimensional interconnected hierarchical porous structure, is employed as a host for lithium (Li) anodes.
2. The functions of wood hosts are systematically evaluated across different battery configurations. The porous structure of wood enables it to homogenize the electric field intensity near the anode, thereby regulating the Li plating/stripping behavior. As a result, wood hosts lead to longer lifespans and lower polarization voltages of batteries. By leveraging the distinctive characteristics of natural wood structures, an all-wood-based Li|S full coin cell is also assembled.
3. Future work could focus on enhancing the electrochemical performances of wood hosts through post-modification. Additionally, there is potential to further expand the range of battery systems utilizing wood.

Introduction

Rechargeable batteries, as one of the most important energy storage devices, are experiencing flourishing development due to the increasing demand for storing intermittent renewable energy and rapid evolution of electrical devices and electric vehicles. Although lithium-ion batteries (LIBs) have achieved major success and have been widely used, the energy density of LIBs is approaching the theoretical limit.[1] To this end, there is an urgent need to develop rechargeable battery systems with higher energy density. By virtue of its ultrahigh theoretical specific capacity (3860 mA h g^{-1}) and low reduction potential (−3.04 V *vs.* standard hydrogen electrode), lithium (Li) metal stands out as an advanced anode material.[2–4] Also, it provides lithium metal batteries (LMBs) with higher energy density than LIBs as promising candidates for next-generation energy storage systems.[5,6] However, the practical use of Li anodes has faced challenges on account of the non-uniform behavior of Li plating/stripping, leading to severe dendrite growth and

[a]*College of Bioresources Chemical and Materials Engineering, Shaanxi University of Science & Technology, Xi'an 710021, P. R. China. E-mail: chenwj4985@sust.edu.cn*
[b]*Beijing Key Laboratory of Lignocellulosic Chemistry, Beijing Forestry University, Beijing 100083, P. R. China*
[c]*Beijing Key Laboratory of Green Chemical Reaction Engineering and Technology, Department of Chemical Engineering, Tsinghua University, Beijing 100084, P. R. China*
[d]*Science and Education Integration College of Energy and Carbon Neutrality, Zhejiang University of Technology, Hangzhou 310011, P. R. China*
† Electronic supplementary information (ESI) available. See DOI: https://doi.org/10.1039/d4gc05507a

volume expansion, which further induce rapid lifespan decay and even safety hazards of LMBs.[7–9]

Different from the insertion-host electrode (carbon, silicon, oxide, *etc.*), the hostless structure of the Li anode leads to random Li plating/stripping, leading to uncontrollable Li dendrite growth and virtually unlimited expansion of the Li anode.[10,11] Therefore, introducing Li metal into a host is expected to solve the mentioned issues effectively.[12,13] Nowadays, various types of Li hosts have been developed, including Li alloy-based,[14,15] metal-based,[16,17] carbon-based,[18,19] and polymer-based hosts.[20–22] Despite the diverse materials used, a common characteristic among these hosts is a three-dimensional (3D) structure with interconnecting pores.[23,24] This structural feature plays a crucial role in regulating the Li plating/stripping behavior, inhibiting dendrite growth, and mitigating volume fluctuations of the Li anode.[25]

Actually, there are many 3D porous structural materials in nature, of which the most representative is wood, *i.e.*, the secondary xylem of trees.[26] As the basic morphological unit of wood, the growth of a wood cell begins at the vascular cambium, and progresses through stages of cell division, cell expansion, cell wall thickening, and finally programmed cell death.[27] The cell wall, which is the solid structure of a wood cell, is primarily composed of cellulose, hemicellulose, and lignin. The interactions among these components *via* hydrogen bonds and chemical bonds (such as ester and ether bonds) create a reinforced concrete structure that affords excellent mechanical strength to the wood cell.[28] This self-assembled highly interconnected hierarchical porous structure of wood attracts significant attention. According to Thygesen *et al.*,[29] the macro-voids in wood, which range in diameter from 10 to 400 μm, include lumens of hardwood vessels and softwood tracheids. The microvoids encompass pit apertures, pit-membrane voids, and other small voids with diameters ranging from 10 nm to 10 μm. Moreover, there are numerous nanovoids among the microfibrils in wood cell walls, typically with diameters smaller than 10 nm. This intricate natural porous structure facilitates the intercellular transport of water, nutrients, and gases (such as oxygen and carbon dioxide) essential for supporting the physiological processes of trees.[30,31] The unique structure identified earlier equips wood with potential as a host for Li metal by offering sufficient space to accommodate deposited Li, ample strength to mitigate the volume expansion of the Li anode during cycles, and a network of pores and channels to facilitate ion transport. Although some researchers have proposed Li hosts mimicking the bionic structure of wood, direct integration of natural wood into LMBs is yet to be explored.

In this contribution, natural wood with a 3D interconnected hierarchical porous structure is employed as a Li host. The wood/Li composite anode is fabricated through a facile rolling method, and is paired with different cathodes of $LiFePO_4$ (LFP) and sulfur (S), respectively. The use of a wood host is proved to homogenize the electric field intensity near the Li anode, thereby regulating the homogeneity Li ion flux and preventing the formation of Li dendrites. Furthermore, the unique 3D structure of the wood host is demonstrated to be capable of accommodating the deposited Li. Consequently, the wood/Li composite anode demonstrates reduced polarizations and longer cycling lifespans in both Li|LFP and Li|S full coin cells compared to anodes without the wood host. In order to further explore the potential of the natural wood structure, an all-wood-based Li|S full coin cell is constructed, comprising a wood/Li composite anode, wood/S cathode, and wood separator.

Results and discussion

Eucalyptus, a fast-growing hardwood that is widespread in southern China, was chosen as the raw material for the Li host. The wood sample was dewaxed first to remove the organic solvent extractions and only the cell wall was retained as the framework, which was conducive to adequately exposing the interconnected pores and channels. Subsequently, the wood sample was sliced along the transverse section as shown in Fig. 1a, resulting in wood slices with a thickness ranging from 50 to 100 μm that maintained adequate flexibility, as depicted in Fig. 1b, and could be rolled up without deformation. The mercury intrusion method was performed to characterize the porous structure of wood slices, especially the mesopores and macropores (Fig. 1c). This showed that the porosity of eucalyptus is 67.6%, indicating the highly porous structure of wood. The maximum mercury intake is observed at 30 μm, with a sub-peak at 90 μm, corresponding to the cell lumens of fiber and vessel cells, respectively.

The wood/Li composite anode was fabricated using a rolling process of a wood slice and Li foil as illustrated in Fig. 2a. A digital picture of the wood/Li composite anode is exhibited in Fig. 2b. After rolling, the Li metal is filled into the

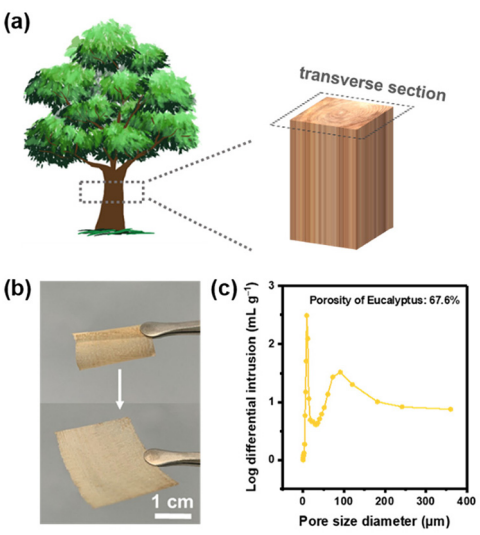

Fig. 1 (a) Schematic illustration for wood slice preparation. (b) Digital picture of the wood slice. (c) Pore size distribution and porosity of eucalyptus wood obtained by the mercury intrusion method.

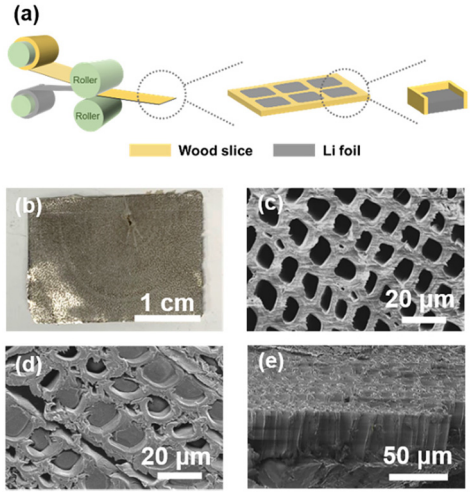

Fig. 2 (a) Schematic diagram for wood/Li composite anode with the rolling process. (b) Digital picture of the wood/Li composite anode. SEM images of (c) eucalyptus wood and (d and e) wood/Li composite anodes.

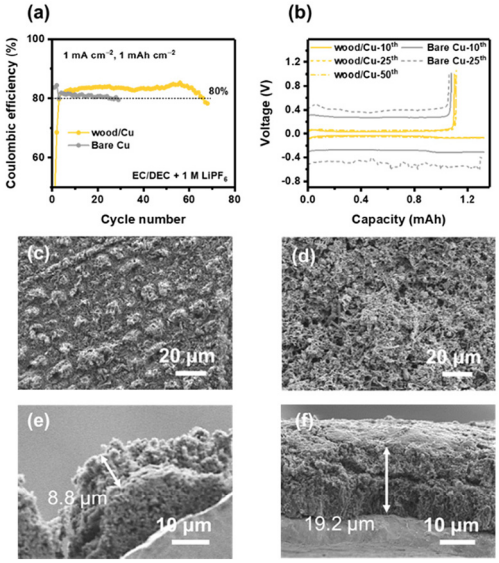

Fig. 3 Electrochemical performances of Li|Cu half cells at 1.0 mA cm^{-2} and 1.0 mA h cm^{-2}: (a) coulombic efficiency values during cycling and (b) charging–discharging curves at different cycles. Morphologies of deposited Li after 5 cycles in Li|Cu half cells with (c and e) or without (d and f) the wood host.

initially hollow cell lumens under pressure (Fig. 2c), and is well confined by the cell walls, as depicted in Fig. 2d. Notably, the wood host retains its structural integrity without significant crushing after rolling because of the sufficient mechanical strength provided by the cell walls, as evidenced by the cross-sectional scanning electron microscope (SEM) image of the composite anode and the 3D morphology observed *via* X-ray microscopy, presented in Fig. 2e and Fig. S1,† respectively. Three types of anodes with varying capacities were prepared by rolling wood slices and Li foils of different thicknesses (50, 75, and 100 μm). After a deep delithiation at 0.5 mA cm^{-2} to 0.5 V (*vs.* Li/Li^+), the composite anodes showed discharging capacities of 9.94, 14.14, and 21.38 mA h cm^{-2}, respectively (Fig. S2†). This demonstrates that the wood host does not affect the Li metal capacity (0.2 mA h cm^{-2} μm_{Li}^{-1}).[24] Furthermore, on subjecting the wood/Li composite anode (50 μm) to a 90% delithiation test at 1.0 mA cm^{-2}, it was found that the structural channels of the wood host remained intact, indicating the robust mechanical stability of the wood hosts (Fig. S3†).

To investigate whether the wood host is beneficial for regulating Li plating/stripping, Li nucleation overpotential was evaluated first.[32] As shown in Fig. S4,† the wood/Cu electrode displayed a significantly low overpotential of 13.0 mV at the nucleating stage compared to the bare Cu electrode, which recorded an overpotential of 94.9 mV. This result indicates that the intricate porous structure of natural wood aids the nucleating–depositing process. Additionally, the abundant pores in the wood, once fully infiltrated with the electrolyte, facilitate ion transportation, leading to a lower overpotential. Subsequently, the efficacy of the wood hosts was probed in cycling Li|Cu half cells. Adopting a coulombic efficiency (CE) of 80% as the benchmark, the wood/Cu electrode demonstrated a retention of more than 66 cycles, while the bare Cu electrode exhibited obvious CE decay after only 25 cycles (Fig. 3a). The charging/discharging polarization curves depicted in Fig. 3b reveal that the wood/Cu electrode exhibits lower polarization voltages throughout the cycling process, registering values of only 70.9 and 76.6 mV at the 10^{th} and 25^{th} cycle, respectively. Notably, a mere increase of 31.9 mV is observed at the 50^{th} cycle. In contrast, the Cu electrode displays substantially higher polarization voltages, recording 547.9 mV at the 10^{th} cycle, which is 7.7 times greater than that of the wood/Cu electrode. Moreover, at the 25^{th} cycle, the polarization voltage for the Cu electrode surges to 942.7 mV, and the fluctuation discharging profile illustrates the uneven Li plating behavior in the absence of the wood host. The morphologies of the cycled wood/Cu and bare Cu electrodes were further investigated by SEM characterization. After 5 cycles at 1.0 mA h cm^{-2} and 1.0 mA cm^{-2}, the wood/Cu electrode exhibited a compact and uniform array of deposited Li, which is attributed to the deposition of Li within the pores of the wood host (Fig. 3c). Conversely, the Li deposition on the bare Cu electrode appears more disordered and looser (Fig. 3d). Furthermore, the thickness of the deposited Li on the wood/Cu electrode is only 8.8 μm, which is less than half of the Li deposition thickness on the bare Cu electrode (19.2 μm) (Fig. 3e and f). This observation underscores that the wood host effectively mitigates the volume expansion associated with deposited Li, thereby promoting a more uniform and stable Li plating/stripping process.

To verify the long-term stability of the wood/Li composite anode, Li|Li symmetrical cells were assembled. As illustrated in Fig. S5a,† the wood/Li composite electrode demonstrates stable cycling performance for over 225 hours (1 mA cm^{-2},

1 mA h cm^{-2}), which exceeds that of the bare Li electrodes by 50 hours. Furthermore, as depicted in Fig. S5b,† the wood/Li composite electrode maintains significantly lower polarization voltages throughout the entire cycling process. After cycling, deposited Li is observed in the pores of the wood host (Fig. S6a and b†). In contrast, the morphology of the Li electrode without the wood host appears more chaotic and disordered (Fig. S6c†). The surface SEM images of the cycled wood/Li electrode demonstrate the role of the wood host in inducing Li deposition.

Apart from eucalyptus, other species of wood were also used as hosts for the Li anode, including Paulownia (abbreviated to Pau), Fir, Pine and Balsa. Using the same method, composite Li anodes were prepared with different wood hosts. As shown in Fig. S7,† the Li metal is successfully filled into numerous cell lumens except for in the Balsa wood. In the case of Balsa wood, the insufficient mechanical strength leads to the crushing of cell walls under pressure during rolling. Additionally, the performances of Li|Cu half cells with different wood hosts were also assessed. All the electrodes employing wood hosts demonstrate a stable CE of around 80% for more than 54 cycles at 1.0 mA h cm^{-2} and 1.0 mA cm^{-2} (Fig. S8†). The experiments for the expansion of wood species illustrate the broad applicability of utilizing wood as a host for Li anodes. The natural interconnected porous structure of wood is highlighted as a critical element in influencing the behavior of Li plating/stripping, thereby contributing to enhanced cycling stability characterized by improved CE and reduced polarization.

Finite element simulation was employed to further understand the mechanism of the wood host (Fig. 4a). Models of Li|Li symmetric cells with or without the wood host were constructed, and the electric field distributions near the surfaces of the Li anodes were compared (Fig. 4b). The electric field intensity near the bare Li anode surface exhibited significant fluctuations due to the presence of a porous polypropylene separator, with a simplified structure of 20 μm thickness and regular pores of 200 nm. Undoubtedly, the inhomogeneous electric field will cause uneven Li deposition, resulting in issues such as Li dendrites, volume expansion, increased polarizations, and rapid lifecycle decay.[33,34] Conversely, after introducing the insulating wood host, the electric field intensity is observed to be more uniformly distributed, promoting a more homogeneous Li deposition within the cell lumens.

To further demonstrate the application potential of the wood/Li composite anode, Li|LFP and Li|S full cells were assembled respectively, utilizing a 50 μm eucalyptus wood host and 50 μm Li. During the early cycling stage at 0.5 C (1 C = 170 mA g^{-1}), both cells, one with the wood/Li composite anode and the other with the bare Li anode, exhibit steady and comparable discharging capacities, as depicted in Fig. S9a.† The cell featuring the wood/Li composite anode maintains a capacity retention of 77.5% after 100 cycles, surpassing the 68.0% retention of the cell with the bare Li anode. Additionally, the polarization voltage of the cell with the wood/Li composite anode is smaller than that of the cell with a bare Li anode at the 100th cycle (Fig. S9b†). Subsequently, as the cycling rate increases to 1.0 C, the Li|LFP cell with the bare Li anode demonstrates a marked capacity decline after 80 cycles, resulting in a capacity retention of only 71.4% after 100 cycles (Fig. 5a). Concurrently, the CE also fades and fluctuates after 80 cycles, illustrating limitations in the availability of active Li. In contrast, the wood/Li composite anode facilitates a more stable cycling behavior, exhibiting not only a higher CE, but also an impressive capacity retention of 98.2% after 100 cycles, which is 26.8% higher than that of the cell with bare Li. Notably, the cell with the composite anode maintains lower polarization voltages through the cycling process, with a value of 245.5 mV at the 10th cycle, and a modest increase of 126.8 mV at the 80th cycle. However, the polarization voltage of the cell with a bare Li anode surges by nearly 200.0 mV within the same cycling period (Fig. 5b). The cells were disassembled after long cycling at 1.0 C. It was shown that the bare Li anode was seriously pulverized (Fig. S10a†). In comparison, the

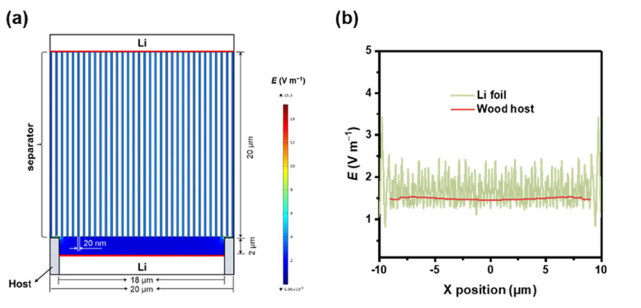

Fig. 4 (a) Electric field intensity distribution in Li|Li symmetrical cells with the wood host. (b) Electric field intensity distribution around the surface of the wood/Li anode.

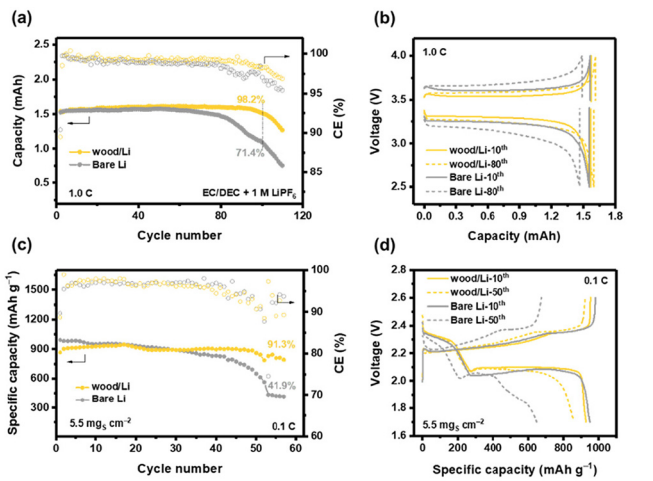

Fig. 5 Electrochemical performances of Li|LFP full cells: (a) long-term cycling performances at 1.0 C and (b) charging–discharging curves at the 10th and the 80th cycle, respectively. Electrochemical performances of Li|S full cells with high sulfur areal loading, (c) long-term cycling performances and (d) charging–discharging curves at the 10th and the 50th cycle, respectively.

wood/Li composite anode still retained structural integrity (Fig. S10b†), demonstrating the long-term stability of the composite anode.

The electrochemical performances of Li|S full cells were evaluated under mild conditions with low sulfur loading cathodes at first. After 200 cycles at 0.5 C (1 C = 1672 mA g^{-1}), the cell with a wood/Li anode shows 70.8% capacity retention, slightly higher than that of the cell with a bare Li anode (65.4%) (Fig. S11a†). Notably, the enhanced cycling stability is further highlighted at 1.0 C. Specifically, the cell equipped with a wood/Li composite anode demonstrates a capacity retention of 75.6% after 250 cycles, representing a substantial improvement of 31.3% compared to the control group (Fig. S11c†). Beyond mitigating capacity degradation, the wood host is also conducive to reducing polarization voltages, especially at the end of the cycling (Fig. S11b and S11d†). Subsequently, when the wood/Li composite anodes were paired with cathodes of high sulfur loading (5.5 mg_S cm^{-2}), the full cells also exhibited superior cycling performances. Although the initial specific capacity of the cell with the bare Li anode exceeds that of the wood/Li composite anode, it shows a rapid decay (Fig. 5c). In contrast, the cell employing the wood/Li composite anode achieves a remarkable capacity retention of 91.3% by the 57th cycle, a significant improvement of almost 50% compared to the cell with the bare Li anode (41.9%). The charging–discharging profiles depicted in Fig. 5d, reveal comparable polarization voltages of the two cells at the 10th cycle. However, the noticeable inclination in the discharging curve of the cell with a bare Li anode at the 50th cycle indicates the failure of the anode.[35,36] After introducing the wood host, the cell still maintains an intact discharging curve with two distinct platforms even after 50 cycles, with a modest increase in polarization voltage of only 38.9 mV from the 10th to the 50th cycle. The consistent results observed in both Li|LFP and Li|S full cells demonstrate that the composite anode integrated with a natural wood host can effectively attenuate polarization voltages and promote long-term cycling stability.

The abundant and interconnected pores make wood not only an excellent host material for Li, but also an ideal framework for active materials of the cathode.[37] For example, Li *et al.* employed carbonized Balsa wood loaded with a catalyst as the cathode of Li–air batteries.[38] To fabricate self-standing wood/S cathodes, the wood slices were first carbonized at 900 °C and then impregnated with a sulfur/carbon (S/C) slurry under vacuum. The S/C compounds are successively filled into the cell lumens as well as the channels (Fig. S12a and S12b†), and the thickness of the wood/S cathode is approximately 257 μm with a sulfur loading of 4.5 mg (Fig. S12c†). Paired with a Li anode of 600 μm thickness, the performances of the wood/S cathode were evaluated first. As shown in Fig. S13a,† the specific capacities at the 1st and the 100th cycle are 893.0 and 552.0 mA h g^{-1}, respectively. Also, the CE remains above 98.5% throughout cycling. The discharging curves at the 1st and the 80th cycle both exhibit the typical two platforms of a Li|S cell, with the voltages of the 2nd platform exceeding 2.0 V

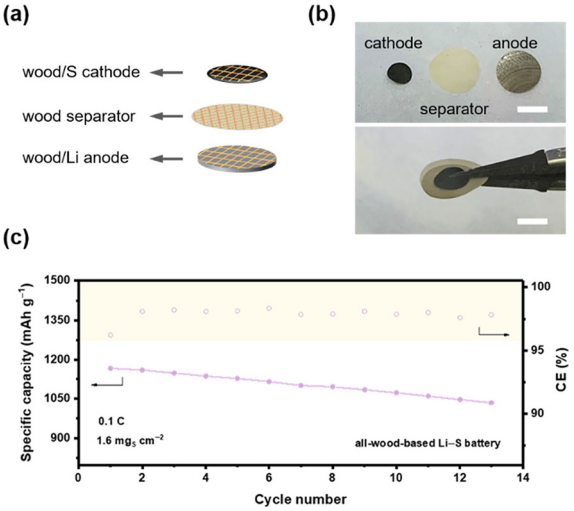

Fig. 6 (a) Schematic illustration of the all-wood-based Li|S full cell. (b) Digital pictures of wood/S, wood/Li and wood separator (the scale bar is 1 cm). (c) Cycling performance of the all-wood-based Li|S full cell.

(Fig. S13b†). These results illustrate that the carbonized wood frameworks are capable of affording stable cycling of the wood/S cathodes. In a battery, a separator is crucial for preventing short circuits by separating the anode and cathode.[39,40] A separator with sufficient porosity is essential for ion transport.[41,42] The abundant interconnecting pore structures of natural wood can be employed as ion transport channels, endowing wood with potential as a separator in batteries. Yang *et al.* reported a modified wood separator for Li-ion batteries with good performances, but there has been no attempt at using a natural wood separator in a more complicated battery system, such as Li–S batteries.[43] Considering that the diameters of the pores in the transverse section of wood are too large to isolate the anode and the cathode, wood slices (100 μm in thickness) along the radial section were prepared as separators in this work. In this way, the wood separator can not only prevent short circuits, but also ensure ion transport through the preserved micro and nano pores (Fig. S14†). Employing the as-prepared wood/Li composite anode, wood/S cathode, and wood separator, an all-wood-based Li|S full cell was constructed (Fig. 6a and b). With a sulfur loading of 1.6 mg_S cm^{-2}, the cell exhibits a specific capacity of 1165 mA h g^{-1} at the 1st cycle and 1034 mA h g^{-1} at the 13th cycle, respectively (0.1 C), maintaining a CE of over 97% during cycling (Fig. 6c).

Conclusions

Natural wood was utilized as a Li host due to its elaborate 3D structure with abundant and interconnecting pores. The wood host contributes to a more uniform electric field intensity distribution near the Li anode, consequently aiding in the regulation of Li plating/stripping. When employed in Li|Cu half

cells, the wood host enables a low Li nucleating overpotential of only 13.3 mV, a more stable cycling ability, a regular patterned Li deposition morphology, and diminished volume expansion. The effectiveness of wood/Li composite anodes is further demonstrated in Li|LFP and Li|S full cells. Specifically, the wood/Li|LFP cell maintains a capacity retention of 98.2% after 100 cycles at 1.0 C, representing a 26.8% improvement compared to a cell with a bare Li anode. Additionally, when paired with high sulfur loading cathodes, the wood/Li|S full cells achieve nearly 50% higher capacity retention than bare Li|S cells. Moreover, the natural structure of wood allows it to be utilized for separators and frameworks for cathodes in batteries. An all-wood-based Li S full cell is constructed and it achieves a discharge capacity exceeding 1000 mA h g^{-1} during cycling. This study successfully showcases the potential of natural wood with an interconnecting porous structure in regulating Li plating/stripping processes and is expected to provide some references for the structural design of materials in rechargeable batteries. In the future, modifications of the natural wood host, such as introducing some lithiophilic sites or functional groups, beneficial for a stable solid electrolyte interphase, are expected for further improving the electromechanical performances.

Data availability

All data generated or analysed during this study are included in this published article and its ESI.†

Conflicts of interest

There are no conflicts to declare.

Acknowledgements

This work was supported by the National Natural Science Foundation of China (22308208) and the Foundation (no. KF202101) of Key Laboratory of Pulp and Paper Science & Technology of Ministry of Education, Qilu University of Technology (Shandong Academy of Sciences).

References

1 Z. Zhu, T. Jiang, M. Ali, Y. Meng, Y. Jin, Y. Cui and W. Chen, *Chem. Rev.*, 2022, **122**, 16610–16751.
2 Z. Han, C. Zhang, Q. Lin, Y. Zhang, Y. Deng, J. Han, D. Wu, F. Kang, Q.-H. Yang and W. Lv, *Small Methods*, 2021, **5**, 2001035.
3 R. K. Petla, I. Lindsey, J. Li and X. Meng, *ChemSusChem*, 2024, e202400281.
4 Y. Du, X. Gao, S. Li, L. Wang and B. Wang, *Chin. Chem. Lett.*, 2020, **31**, 609–616.
5 S. Kim, G. Park, S. J. Lee, S. Seo, K. Ryu, C. H. Kim and J. W. Choi, *Adv. Mater.*, 2023, **35**, 2206625.
6 A. Patrike, P. Yadav, V. Shelke and M. Shelke, *ChemSusChem*, 2022, **15**, e202200504.
7 X.-B. Cheng, R. Zhang, C.-Z. Zhao and Q. Zhang, *Chem. Rev.*, 2017, **117**, 10403–10473.
8 X. Zhang, Y. Yang and Z. Zhou, *Chem. Soc. Rev.*, 2020, **49**, 3040–3071.
9 T. Hu, Y. Guo, Y. Meng, Z. Zhang, J. Yu, J. Cai and Z. Yang, *Chin. Chem. Lett.*, 2024, **35**, 108603.
10 Z. Zhu, B. Liu, Y. Qian, Y. Fang, X. Lei, X. Liu, J. Zhou, Y. Qian and G. Wang, *Adv. Energy Mater.*, 2022, 2203687.
11 R. Zhang, N.-W. Li, X.-B. Cheng, Y.-X. Yin, Q. Zhang and Y.-G. Guo, *Adv. Sci.*, 2017, **4**, 1600445.
12 W. Guan, X. Hu, Y. Liu, J. Sun, C. He, Z. Du, J. Bi, K. Wang and W. Ai, *Research*, 2022, **2022**, 1–16.
13 C. Jin, O. Sheng, M. Chen, Z. Ju, G. Lu, T. Liu, J. Nai, Y. Liu, Y. Wang and X. Tao, *Mater. Today Nano*, 2021, **13**, 100103.
14 Q. Yun, Y.-B. He, W. Lv, Y. Zhao, B. Li, F. Kang and Q.-H. Yang, *Adv. Mater.*, 2016, **28**, 6932–6939.
15 D. Chen, P. Qing, F. Tang, H. Yu, P. He, H. Huang, Z. Wu, F. Sun, W. Wei, X. Ji and L. Chen, *Mater. Today Energy*, 2023, **33**, 101272.
16 L. Ye, P. Feng, X. Chen, B. Chen, K. Gonzalez, J. Liu, I. Kim and X. Li, *Energy Storage Mater.*, 2020, **26**, 371–377.
17 W. Chen, S. Li, C. Wang, H. Dou and X. Zhang, *Energy Environ. Mater.*, 2023, **6**, e12412.
18 H. Chen, Y. Yang, D. T. Boyle, Y. K. Jeong, R. Xu, L. S. de Vasconcelos, Z. Huang, H. Wang, H. Wang, W. Huang, H. Li, J. Wang, H. Gu, R. Matsumoto, K. Motohashi, Y. Nakayama, K. Zhao and Y. Cui, *Nat. Energy*, 2021, **6**, 790–798.
19 T. Wei, J. Lu, P. Zhang, Q. Zhang, G. Yang, R. Yang, D. Chen, Q. Wang and Y. Tang, *Chin. Chem. Lett.*, 2024, **35**, 109122.
20 J. Jiang, Z. Pan, Z. Kou, P. Nie, C. Chen, Z. Li, S. Li, Q. Zhu, H. Dou, X. Zhang and J. Wang, *Energy Storage Mater.*, 2020, **29**, 84–91.
21 P. Shi, Z.-Y. Liu, X.-Q. Zhang, X. Chen, N. Yao, J. Xie, C.-B. Jin, Y.-X. Zhan, G. Ye, J.-Q. Huang, S. Ifan E L, T. Maria-Magdalena and Q. Zhang, *J. Energy Chem.*, 2022, **64**, 172–178.
22 P. Shi, X. Zhang, X. Shen, B. Li, R. Zhang, L. Hou and Q. Zhang, *Adv. Funct. Mater.*, 2021, **31**, 2004189.
23 H. Wang, D. Lin, J. Xie, Y. Liu, H. Chen, Y. Li, J. Xu, G. Zhou, Z. Zhang, A. Pei, Y. Zhu, K. Liu, K. Wang and Y. Cui, *Adv. Energy Mater.*, 2019, **9**, 1802720.
24 P. Shi, T. Li, R. Zhang, X. Shen, X.-B. Cheng, R. Xu, J.-Q. Huang, X.-R. Chen, H. Liu and Q. Zhang, *Adv. Mater.*, 2019, **31**, 1807131.
25 Y. Cheng, J. Chen, Y. Chen, X. Ke, J. Li, Y. Yang and Z. Shi, *Energy Storage Mater.*, 2021, **38**, 276–298.
26 C. Chen, Y. Kuang, S. Zhu, I. Burgert, T. Keplinger, A. Gong, T. Li, L. Berglund, S. J. Eichhorn and L. Hu, *Nat. Rev. Mater.*, 2020, **5**, 642–666.

27 L. Salmén, in *Plant Biomechanics: From Structure to Function at Multiple Scales*, Springer, Cham, 2018, pp. 3–19.
28 L. Luo and L. Li, *For. Res.*, 2022, **2**, 1–11.
29 L. G. Thygesen, E. Tang Engelund and P. Hoffmeyer, *Holzforschung*, 2010, **64**, 315–323.
30 B. Hui, K. Zhang, Y. Xia and C. Zhou, *Electrochim. Acta*, 2020, **330**, 135274.
31 F. Wang, J. Lee, L. Chen, G. Zhang, S. He, J. Han, J. Ahn, J. Y. Cheong, S. Jiang and I.-D. Kim, *ACS Nano*, 2023, **17**, 8866–8898.
32 X. Yan, Q. Zhang, W. Xu, Q. Xie, P. Liu, Q. Chen, H. Zheng, L. Wang, Z.-Z. Zhu and D.-L. Peng, *J. Mater. Chem. A*, 2020, **8**, 1678–1686.
33 H. Liu, C. Yang, M. Han, C. Yu, X. Li, Z. Yu and J. Qu, *Angew. Chem., Int. Ed.*, 2023, **62**, e202217458.
34 I. Yang, J. Jeong, J. Y. Seok and S. Kim, *Adv. Energy Mater.*, 2023, **13**, 2202321.
35 L.-P. Hou, L.-Y. Yao, C.-X. Bi, J. Xie, B.-Q. Li, J.-Q. Huang and X.-Q. Zhang, *J. Energy Chem.*, 2022, **68**, 300–305.
36 L.-P. Hou, X.-Q. Zhang, N. Yao, X. Chen, B.-Q. Li, P. Shi, C.-B. Jin, J.-Q. Huang and Q. Zhang, *Chem*, 2022, **8**, 1083–1098.
37 Y. Li, K. (Kelvin) Fu, C. Chen, W. Luo, T. Gao, S. Xu, J. Dai, G. Pastel, Y. Wang, B. Liu, J. Song, Y. Chen, C. Yang and L. Hu, *ACS Nano*, 2017, **11**, 4801–4807.
38 J. Li, Y. Cai, Y. Zhai and X. Sun, *Appl. Surf. Sci.*, 2024, 162204.
39 Y. Hu, X. Zhu and L. Wang, *ChemSusChem*, 2020, **13**, 1366–1378.
40 M. Zhang, X. Zhang, S. Liu, W. Hou, Y. Lu, L. Hou, Y. Luo, Y. Liu and C. Yuan, *ChemSusChem*, 2024, e202400538.
41 B. Boateng, X. Zhang, C. Zhen, D. Chen, Y. Han, C. Feng, N. Chen and W. He, *Nano Sel.*, 2021, **2**, 993–1010.
42 L. Ding, D. Li, L. Liu, P. Zhang, F. Du, C. Wang, D. Zhang, S. Zhang, S. Zhang and F. Yang, *J. Energy Chem.*, 2023, **84**, 436–447.
43 Y. Yang, N. Li, T. Lv, Z. Chen, Y. Liu, K. Dong, S. Cao and T. Chen, *Nanoscale Adv.*, 2022, **4**, 1718–1726.